CEAS EuroGNC 2019

CEAS-GNC-2019-063

"Conference on Guidance, Navigation and Control"

3-5 April 2019 @ Politecnico di Milano, Milan, Italy.

POLITECNICO
MILANO 1863

Design and Assessment of a Two Degree of Freedom Gust Load Alleviation System

Daniel Ossmann and Charles Poussot-Vassal

Abstract The design and assessment of a two degree of freedom gust load alleviation control system for a business jet aircraft is presented in this paper. The two degrees of freedom are a disturbance estimator to compute the incoming gusts as well as a feedback control law to mitigate the estimated disturbance to reduce the aircraft loads. To facilitate the estimator design, high order, infinite-dimensional models of the structural and aerodynamic aircraft dynamics are approximated by low order models using advanced model reduction techniques. For the robust disturbance estimator design an innovative approach relying on nullspace-based techniques together with non-linear optimization is proposed. Time delays, originating from the aerodynamics modeling, the discrete control loop, and the sensor and actuator dynamics, play a key role in the stability and performance assessment of a gust load alleviation controller. Thus, a novel analytical analysis method is presented to explicitly evaluate the influence of these time delays on the closed loop. Finally, the developed tool-chain is applied to a fly-by-wire business jet aircraft. The resulting two degrees of freedom gust load alleviation system is verified in a simulation campaign using a closed loop, non-linear simulator of the aircraft.

1 Introduction

In order to allow for a more economic and environmentally friendly aircraft operation and to fulfill the greener imperative demanded by today's society, fuel savings and cost reduction play a key role in the development of modern aircraft. Besides

_____

Dr. Daniel Ossmann

Institute of System Dynamics and Control, German Aerospace Center, Muenchener Strasse 20, 82234 Wessling, Germany, e-mail: `Daniel.Ossmann@dlr.de`

Dr. Charles Poussot-Vassal

Systems and Signal Processing Department, ONERA Centre de Toulouse, 2 Avenue Edouard Belin, 31000 Toulouse, France, e-mail: `Charles.Poussot-Vassal@onera.fr`

the efficiency of engines and aerodynamics, the aircraft weight has a major impact on fuel consumption [11]. Thus, reducing structural loads on an aircraft by using advanced active control techniques is a main research interest of today's aircraft industry. Reducing the loads allows the aircraft manufacturer to build and certify [6] the aircraft for a smaller load envelope, which inherently reduces the structure of the aircraft and reduced fuel and costs, see [12] for a realistic example. The loads itself arise from steering the aircraft (maneuver loads) and from external disturbance inputs (gust loads). Considering new aircraft configurations with improved lift-to-drag ratios, a special focus is put on gust load alleviation, as these aircraft are prone to have an increased sensitivity to atmospheric disturbances. A well written overview of state-of-the-art gust load alleviation approaches and aircraft featuring active gust load alleviation systems is provided in [24].

In this paper we present a tool chain to develop a two degrees of freedom gust load alleviation system for a given aircraft configuration to reduce the gust loads. The gust load alleviation controller features a disturbance estimator to estimate the incoming gusts and a dedicated controller to reduce the gust effects. The two degrees of freedom system purely works in the feedback path using already available measurements on the aircraft. Feed-forward control using additional sensors (e.g, LIDAR) is not considered herein. Interested readers in such based methods are referred to [14, 13] as well as [7] presenting a combination of feed forward and feedback techniques are presented.

A main difference between a classical flight control design and the design of a gust load alleviation system is, that for the latter usually complex, high order models are available, which allow the determination of the forces and moments on the aircraft structure. Such models need to include detailed descriptions of the aircraft structure as well as the steady and unsteady aerodynamics, leading to high order models. As the aircraft structure is often decomposed in several sections to better reflect the impact of the gust moving along the aircraft, time delays need to be included in the model as well. These complex models are not well suited for the control design. Thus, in Sect. 2 a method to approximate these infinite-dimensional models by low order finite-dimensional models is presented. In Sect. 3 an advanced approach to design a robust disturbance estimator, which is robust to parametric uncertainties in the flight envelope, is proposed. As the time delays are approximated in Sect. 2, a dedicated stability analysis methodology to assess the developed gust load alleviation system against these delays is derived in Sect. 4. This intermediate step is to be performed before the classical verification of the gust load alleviation system in simulation. Fig. 1 summarizes the proposed tool-chain with the herein presented novel design techniques (highlighted in bold). The presented tool-chain is applied to develop a gust load alleviation controller for a generic example of a medium size business jet in Sect. 5. The latest results of a simulation-based load verification campaign including the comparison to the loads without the gust load alleviation control are reported.
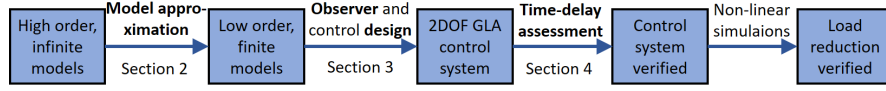
Fig. 1 Proposed tool-chain using advanced mathematical methods for developing a gust load alleviation control system.

2 Model Approximation

When dealing with industrial problems such as aircraft systems, associated models usually embed unsteady aerodynamics as well as structural modes and aerodynamical delays. Consequently, the dimension of the state-space models can be very large and can include a mix of differential and algebraic equations. Thus, before the methods presented in Sect. 3 can be applied, a pre-processing step, to reduce the state dimension and simplify the complexity should be applied first in order to improve the numerical treatment and accuracy of the results. A short reminder of the methods involved in Sect. 5 are discussed below. As these methods are not the main topic of this paper, more details on infinite-dimensional or data-driven model approximation techniques can be found in [1, 5], and on finite order large-scale model approximation in [2, 10]. Let us follow these two classes of problems and remind the driving ideas as follows.

2.1 Infinite-Dimensional/Data-Driven Model Approximation

Given an infinite-dimensional model H, it is possible to obtain the frequency-domain responses $\Phi_i \in \mathbb{C}^{n_y \times n_u}$ for different frequency samples ω_i $(i = 1, \ldots, N)$. Then, one can write $H(\iota \omega_i) = \Phi_i$. One of the data-driven approach is based on the interpolation framework well defined in [17, 1], involving the Loewner matrices. The method consists of an *exact rational model interpolation*, optionally followed by a *reduction procedure*. To this aim, let us first partition the collected data $(\omega_i, \Phi_i)_{i=1}^{N}$ in two disjoint sets as follows ($N = q + k$):

$$\iota[\omega_1, \ldots, \omega_N] = [\mu_1, \ldots, \mu_q] \cup [\lambda_1, \ldots, \lambda_k]$$
$$[\Phi_1, \ldots, \Phi_N] = [\tilde{v}_1, \ldots, \tilde{v}_q] \cup [\tilde{w}_1, \ldots, \tilde{w}_k]. \tag{1}$$

Then, define $l_j \in \mathbb{C}^{n_y \times 1}$ $(j = 1, \ldots, q)$ and $r_i \in \mathbb{C}^{n_u \times 1}$ $(i = 1, \ldots, k)$ the q left and k right tangential directions. Using these tangential directions, let us define $v_j^* = l_j^* \tilde{v}_j \in \mathbb{C}^{1 \times n_u}$ and $w_i = \tilde{w}_i r_i \in \mathbb{C}^{n_y \times 1}$ the *left* and *right tangential* data directions, respectively. Based on the left interpolation driving frequencies $\{\mu_i\}_{i=1}^{q} \in \mathbb{C}$ with left output or tangential directions $\{l_i\}_{i=1}^{q} \in \mathbb{C}^{n_y}$, producing the left responses $\{v_i\}_{i=1}^{q}$ and right interpolation driving frequencies $\{\lambda_i\}_{i=1}^{k} \in \mathbb{C}$ with right input or tangential directions $\{r_i\}_{i=1}^{k} \in \mathbb{C}^{n_u}$, producing the right responses $\{w_i\}_{i=1}^{k}$, the objective is to find a model transfer function $\tilde{H}$ which is a tangential interpolant of the

data, i.e., satisfies the following left and right interpolation conditions:

$$\left.\begin{array}{cc} l_j^* \tilde{H}(\mu_j) = v_j^* & \tilde{H}(\lambda_i) r_i = w_i \\ \text{for } j = 1, \ldots, q & \text{for } i = 1, \ldots, k \end{array}\right\}. \tag{2}$$

The interpolation problem (2) can be solved thanks to the Loewner framework (see, e.g., [17]). One of the important property of the Loewner approach is that it encodes the minimal McMillian degree of the interpolation model and its minimal realization order n. This then leads to an exact descriptor model interpolating the data, especially useful, when the amount of data is very large.

2.2 Finite-Dimensional Model Approximation

Once an exact interpolation model $\tilde{H}$ has been obtained, with potentially large dimension, a second step then consists in approximating this finite order model with a low dimensional one. One common objective in model approximation consists in finding a reduced-order model that well captures the main original input/output dynamical behavior. To address this objective, the (frequency-limited) $\mathscr{H}_2$-norm mismatch error is commonly used, see, e.g., [10, 31]. The resulting approximation problem consists thus in seeking a low order approximation model $\hat{H}(s)$ of $\tilde{H}(s)$, such that:

$$\hat{H} := \arg \min_{\substack{G \in \mathscr{H}_2^{n_y \times n_u} \\ \text{rank}(G) = r \ll n}} ||\tilde{H} - G||_{\mathscr{H}_2}. \tag{3}$$

Beside the fact that problem (3) is non-convex and non-linear, some conditions have been proposed to reach the so-called *first order optimality conditions* and procedures to ensure that a local (hopefully global) optimum is reached. Moreover, the proposed IRKA and FL-ISTIA algorithms are appropriate to practically tackle these problems (see, e.g., [10, 31] for details). Finally, the derived model $\hat{H}$ can be easily brought into the form (4) by separating the inputs accordingly.

3 Disturbance Estimator Design

In this section a robust disturbance estimator design problem is derived. The proposed approach is a combination of the proposed nullspace-based method for disturbance estimation in [18] and the idea of deriving robust filters via optimization [29, 19]. Thus, in a preliminary step the structure of the disturbance estimator is determined using nullspace-based techniques proposed for the disturbance estimator design in [18] applied on a set of linear design models. The extracted structure from this linear design is then optimized to solve the multi-model design problem applying a non-linear optimization techniques similar to the approaches described in [29, 19] for fault detection filters.

3.1 Problem Formulation

Consider the set of linear models described by the input-output form

$$y^{(i)}(s) = G_u^{(i)}(s)u(s) + G_n^{(i)}(s)n(s) + G_d^{(i)}(s)d(s), \tag{4}$$

where $y^{(i)}(s)$, $u(s)$, and $n(s)$ are the Laplace-transformed vectors of the p-dimensional system output vector $y^{(i)}(t)$, the m_u-dimensional control input vector $u(t)$, and the m_n-dimensional noise vector $n(t)$, respectively. The noise vector includes any non-measurable disturbances, which need to be decoupled from the estimate. $d(s)$ is the Laplace-transformed of the scalar disturbance input $d(t)$ to be estimated. $G_u^{(i)}(s)$, $G_n^{(i)}(s)$, and $G_d^{(i)}(s)$ are the transfer-function matrices (TFMs) from control inputs to outputs, noise inputs to outputs, and disturbance to outputs, respectively. The index (i) is used to describe the set of $i = 1, \ldots, N$ linear models, which are linearized around different trim points.

The design goal is to derive a single linear disturbance estimator $O(s)$, which processes the measurable system outputs $y^{(i)}(t)$ and control inputs $u(t)$ and generates the disturbance estimate $\tilde{d}(t)$. In the input-output form this can be described by

$$\tilde{d}^{(i)}(s) = O(s) \begin{bmatrix} y^{(i)}(s) \\ u(s) \end{bmatrix}, \tag{5}$$

where $O(s)$ is the disturbance estimator TFM. Note that the robustness aspects come into play as we search for a single filter $O(s)$ valid for all the N available design models. The order of $O(s)$ is the dimension of the state vector of a minimal state-space realization of $O(s)$. From the general description in (5) follows the definition of the robust disturbance estimation problem (RDEP): Design a physically realizable, stable, and linear disturbance estimator of the form (5) such that

$$\begin{aligned} &(a) \ \tilde{d}^{(i)} \approx 0 \ \text{when } d = 0 \ \forall \ \{u, n\} \ \text{for } i = 1, \ldots, N \\ &(b) \ \tilde{d}^{(i)} \approx d \ \text{when } d \neq 0 \ \text{ for } \ i = 1, \ldots, N \end{aligned} \tag{6}$$

Note that in (6) an approximated form is used, i.e., the estimate shall approximately be zero for any control and noise inputs. In case of such a multi-model formulation an exact decoupling over all models generally cannot be achieved. The remainder of this section focuses on a strategy how the RDEP can be numerically solved.

3.2 Solving the Robust Disturbance Estimation Problem

The design of the robust disturbance estimator $O(s)$ which allows the estimation of the gust for all N models is done in two steps. In the first step the structure of the disturbance estimator is determined, solving a dedicated disturbance estimation problem (DEP) for each model independently. With "structure of the estimator" we refer to finding elements in the observer state space matrices, which are constant

over all grid points (e.g. zero). In the second step the non-constant values in the matrices are defined as free turning parameters and are tuned using a non-smooth optimization to ensure the required conditions (a) and (b).

3.2.1 Estimator Structure

The structure of the disturbance estimator is determined by solving the DEP [18] for each model individually. In this case the computation relies on nullspace techniques for dynamical systems [30]. Let us first consider the ith-model for which the ith-disturbance estimator

$$\tilde{d}^{(i)}(s) = O^{(i)} \begin{bmatrix} y^{(i)}(s) \\ u(s) \end{bmatrix} \tag{7}$$

can be designed. Inserting the model equation (4) into (7) leads to

$$\tilde{d}^{(i)}(s) = O^{(i)}(s) \begin{bmatrix} G_u^{(i)}(s) \ G_n^{(i)}(s) \ G_d^{(i)}d(s) \\ I_{m_u} \quad 0 \quad 0 \end{bmatrix} \begin{bmatrix} u(s) \\ n(s) \\ d(s) \end{bmatrix}, \tag{8}$$

which describes the ith disturbance estimate $\tilde{d}^{(i)}(s)$ depending on the control, noise and disturbance inputs. If the DEP can be solved exactly, we adapt the requirements (a) and (b) of the RDEP to the DEP following [18] to

$$\begin{aligned} (\tilde{a}) \ &\tilde{d} = 0 \ \text{ when } d = 0 \ \forall \ \{u, n\} \\ (\tilde{b}) \ &\tilde{d} \approx d \ \text{ when } d \neq 0, \end{aligned} \tag{9}$$

demanding an exact decoupling of the control inputs u and the noise n from the disturbance estimate in $(\tilde{a})$ and an approximative estimation of the disturbance d in (b)

Next, the formulated requirements in $(\tilde{a})$ and $(\tilde{b})$ can be transformed into algebraic conditions. The decoupling condition (a) requires that the disturbance estimate $\tilde{d}(s)$ is decoupled from all inputs $u(s)$ and noise $n(s)$. This is equivalent to demanding

$$O^{(i)}(s) \begin{bmatrix} G_u^{(i)}(s) \ G_n^{(i)}(s) \\ I_{m_u} \quad 0 \end{bmatrix} := O^{(i)}(s) G_e^{(i)}(s) = 0. \tag{10}$$

It follows that $O^{(i)}(s)$ needs to be a left annihilator of $G_e^{(i)}(s)$. By deriving a minimal basis $N_l^{(i)}(s)$ for the left nullspace of $G_e^{(i)}(s)$, the design conditions $(\tilde{a})$ can be tackled. For design condition $(\tilde{b})$, the basic constraint

$$O^{(i)}(s) \begin{bmatrix} G_d^{(i)}(s) \\ 0 \end{bmatrix} \neq 0 \tag{11}$$

must be fulfilled to ensure the estimate-ability of the disturbance. If the DEP in (10) and (11) can be solved exactly is based on necessary and sufficient rank criteria. As for realistic design problems this condition is often fulfilled, it is not further dis-

cussed herein. Interested readers are referred to [28, 18, 30]. The required nullspace computation in (10) can be solved readily available using numerical tools [30]. If the DEP is solvable, a disturbance estimator can be constructed from the nullspace basis ensuring (11) as well as the minimal order of the resulting estimator. In this design procedure, the actual dynamics of the estimator are a design freedom, i.e., the poles of the filter can be freely chosen.

At this point of the design approach, the DEP has been solved for each of the N models individually. As the underlying models often exhibit the same model structure, which is assumed for the problem herein, a common estimator structure is extracted, reducing the complexity of the optimization described next.

3.2.2 Parameter Tuning

Having defined the structure of the observe the free parameters P of the estimator $O(s)$ in (5) are selected to be the non-zero elements of the observer's state space matrices. The next task is to optimally tune these free parameters. As criteria a H_∞-norm optimization is selected for which numerical tools in MATLAB are available. The disturbance estimator shall ensure the conditions defined in (6). The goal is to design a single estimator which decouples the control inputs and the noise for all N models. As this can seldom be solved exactly, i.e., the decoupling condition (10) cannot be fulfilled for all N models with a single estimator, we use the reformulation of the problem based on the H_∞-norm. Thus, the decoupling requirement (a) is expressed as multi-model norm condition for $i = 1, \dots, N$ by

$$||O(s)\, G_e^{(i)}(s)||_\infty \approx 0. \tag{12}$$

Similar, the disturbance coupling requirement (b) is reformulated as multi-model model matching problem $i = 1, \dots, N$ as

$$||O(s)\, [G_d^{(i)}(s)\, 0]^T - M(s)||_\infty \approx 0, \tag{13}$$

where $M(s)$ defines the desired estimation dynamics. Finally, to determine the free parameters P of the disturbance estimator $O(s)$ the conditions (12) and (13) are turned into the non-convex, non-smooth optimization problem

$$\min_P \max_i ||O(s,P)\, G_e^{(i)}(s)||_\infty$$
$$\text{s.t. } ||O(s,P)\, [G_d^{(i)}(s)\, 0]^T - M(s)||_\infty < \gamma \tag{14}$$
$$P_{\min} < P < P_{\max},$$

for $i = 1, \dots, N$, where $P_{\min}$ and $P_{\max}$ are the minimum and maximum values of the tuning parameters and γ is a parameter to define the accuracy of the disturbance estimate. The optimization problem in (14) can be solved numerically using standard Matlab tools as for example the `systune` command.

4 Stability Assessment

As mentioned in Sect. 2, the considered aircraft models naturally embed internal as well as input and output delays. Looping outputs to inputs through an observer/controller structure then leads to dynamical models with numerous delays. It is preferred, however, to work on a finite-order approximated model $\hat{H}$ for the estimator and control law design as it enables the use of standard numerical tools. Obviously it is better to assess the closed-loop stability on the original *delayed* model before running numerous simulations. Depending on the number of delays and states equations describing the model, this assessment can become complicated. Up to the authors' knowledge, no standard tools are available to explicitly consider this analysis problem. Thus, we propose a procedure (with partial theoretical proof) to approximate the stability of large-scale multiple-delay dynamical equations.

4.1 Preliminaries and Proposed Algorithm

Stability of a dynamical systems is clearly one of the main property to assess in control theory, numerical simulation, optimization, etc. Without loss of generalities, in the case of "classical"[1] linear time-invariant (LTI) models either described by a set of ordinary differential equations or differential algebraic equations, the stability problem is recast as eigenvalue problem. In this specific case, the number of eigenvalues is finite and its computational complexity is only related to the (E,A) pencil calculation[2]. If instead, the LTI model H has an infinite number of singularities or its realization is not necessarily available, the stability assessment becomes much more tedious. Delay invariant models fall within this category. In these cases, tailored solutions are usually invented to deal with these specificity (e.g. the time-delay stability analysis literature is very important and one may refer to [25, 27, 26, 4]). Let us start by noticing that, delayed equations are meromorphic (real-valued) complex functions given as $H : \mathbb{C} \mapsto \mathbb{C}^{n_y \times n_u}$. Moreover, if H ensures

$$\int_{-\infty}^{\infty} ||H(s)||_F^2 dt < \infty, \tag{15}$$

the meromorphic function is said to be of finite energy and $H \in \mathscr{L}_2$. Then, let us define the input-output stability as follows: a system represented by the transfer function $H(s)$ is said to be input-output $L_\infty - L_2$ stable, if there exists a $c > 0$ such that:

$$||Hu||_{L_\infty} = ||y||_{L_\infty} \le c||u||_{L_2}. \tag{16}$$

In this case, the system is said $\mathscr{L}_2$ stable (or $\mathscr{H}_2$). This consideration, i.e., the complex-valued meromorphic function context, is the starting point for the proposed approach. The corresponding proposed numerical procedure, summarized in algo-

---

[1] By "classical", ones means equipped with the (E,A,B,C,D) realization.

[2] In this case, very efficient tools already exist such as LAPACK.

rithm 1 below, embeds a relative simple but effective, fast and reliable procedure. In the algorithm 1 we first exactly match the original input-output model by a rational model $\tilde{H} \in \mathscr{L}_2$ which guarantees interpolatory conditions. Then, we seek for the best stable approximation $\tilde{H}_s \in \mathscr{H}_2$ of the obtained model $\tilde{H} \in \mathscr{L}_2$. The $\mathscr{L}_2$ distance (inner product) between the interpolated $\tilde{H}$ and stable $\tilde{H}_s$ models is computed next. If this stability index is smaller than a given threshold, then one concludes that $\tilde{H}$ (and consequently H) is stable, and unstable otherwise. In the following we derive some arguments to justify the approach. The authors stress, however, that detailed proofs are subject of ongoing research.

Algorithm 1 $\mathscr{L}_2$ - Meromorphic Function Stability Approximation ($\mathscr{L}_2$-MFSA)

Require: $H \in \mathscr{L}_2$, $\{\omega_i\}_{i=1}^N \in \mathbb{R}_+$, $N \in \mathbb{N}$ and $\varepsilon \in \mathbb{R}_+$
 1: Sample H and obtain $\{\omega_i, \Phi_i\}_{i=1}^N$
 2: Perform an exact Loewner interpolation (as described in Sect. 2) and obtain $\tilde{H}$ equipped with a realization and which ensures interpolatory conditions
 3: Compute $\tilde{H}_s$, the stable rational approximation of $\tilde{H}$, following [15]
 4: Compute the stability index as $S = ||\tilde{H}_s - \tilde{H}||_{\mathscr{L}_2}$
 5: **if** $S < \varepsilon$ **then**
 6:     H is stable
 7: **else**
 8:     H is unstable
 9: **end if**

4.2 Stability Assessment based on the $\mathscr{L}_2$ Inner Product

Let us consider a linear multiple-input multiple-output dynamical system, denoted by H with n_u (*resp.* n_y) $\in \mathbb{N}^*$ inputs (*resp.* outputs), represented by its transfer function $h(s) \in \mathbb{C}^{n_y \times n_u}$. Let $\mathscr{L}_2(\iota\mathbb{R})$ be the Hilbert space of holomorphic functions $F : \mathbb{C} \to \mathbb{C}^{n_y \times n_u}$ which are analytic in the complex plane except on the imaginary axis and for which $\int_{-\infty}^{+\infty} \mathbf{tr}\left(\overline{F(\iota\omega)}F^T(\iota\omega)\right) d\omega < +\infty$. For given $G, H \in \mathscr{L}_2(\iota\mathbb{R})$, the associated inner-product reads:

$$\langle G, H \rangle_{\mathscr{L}_2} = \frac{1}{2\pi} \int_{-\infty}^{+\infty} \mathbf{tr}\left(\overline{G(\iota\omega)}H^T(\iota\omega)\right) d\omega, \tag{17}$$

and the $\mathscr{L}_2(\iota\mathbb{R})$ norm can be explained:

$$||G||_{\mathscr{L}_2} = \left(\frac{1}{2\pi} \int_{-\infty}^{+\infty} ||G(\iota\omega)||_F^2 d\omega\right)^{1/2} = \langle G, G \rangle_{\mathscr{H}_2}, \tag{18}$$

where $||G||_F^2 = \langle G, G \rangle_F$ and $\langle G, H \rangle_F = \mathbf{tr}(\overline{G}H^T)$ are the Frobenius norm and inner-product, respectively. Since only real dynamical systems are considered, it is noteworthy that if $G, H \in \mathscr{L}_2$ are real, then $\langle G, H \rangle_{\mathscr{L}_2} = \langle H, G \rangle_{\mathscr{L}_2} \in \mathbb{R}_+$. By noticing that $\mathscr{H}_2(\mathbb{C}_-)$ is the left half-plane analog of $\mathscr{H}_2(\mathbb{C}_+)$, e.g., $G \in \mathscr{H}_2(\mathbb{C}_-)$ if and only if $G(-s) \in \mathscr{H}_2(\mathbb{C}_+)$. Then $\mathscr{H}_2(\mathbb{C}_-)$ stands as the space of transfer function $H(s)$

whose all the singularities lies in $\mathbb{C}_+$, i.e., the poles of $H(s)$ are all unstable. The space $\mathscr{H}_2(\mathbb{C}_-)$ is called the space of anti-stable models. Now, let us remind the following results, on which we ground the result derivation. The $\mathscr{H}_2(\mathbb{C}_-)$ and $\mathscr{H}_2(\mathbb{C}_+)$ spaces are closed subspaces of $\mathscr{L}_2(\imath\mathbb{R})$ and $\mathscr{L}_2(\imath\mathbb{R}) = \mathscr{H}_2(\mathbb{C}_-) \bigoplus \mathscr{H}_2(\mathbb{C}_+)$. In addition, one can remind that by applying the Laplace transform, denoted as $\mathscr{L}(\cdot)$, over these two spaces, the following bijections are obtained:

$$\mathscr{L}(\cdot) : \mathscr{L}_2^n[0,\infty) \to \mathscr{H}_2(\mathbb{C}_+) \text{ and } \mathscr{L}(\cdot) : \mathscr{L}_2^n(-\infty,0] \to \mathscr{H}_2(\mathbb{C}_-), \qquad (19)$$

which maps the causal and anti-causal time-domain functions. Obviously, (19) shows that every element $H \in \mathscr{H}_2(\mathbb{C}_+)$ (respectively $G \in \mathscr{H}_2(\mathbb{C}_-)$) can be uniquely associated to an element $h \in \mathscr{L}_2^n[0,\infty)$ (respectively $g \in L_2^n(-\infty,0]$). In addition, the following functional analysis theorem shows that the Laplace transform preserves inner product and orthogonality.

Theorem 1 (Plancherel). *Let us consider $h_1, h_2 \in \mathscr{L}_2^n(-\infty,\infty)$, one has*

$$\langle H_1, H_2 \rangle_{\mathscr{L}_2(\imath\mathbb{R})} = \langle \mathscr{L}(h_1), \mathscr{L}(h_2) \rangle_{\mathscr{L}_2(\imath\mathbb{R})} = \langle h_1, h_2 \rangle_{L_2}. \qquad (20)$$

Moreover, since $\mathscr{H}_2(\mathbb{C}_-)$ is orthogonal to $\mathscr{H}_2(\mathbb{C}_+)$ with respect to the $\mathscr{L}_2(\imath\mathbb{R})$-inner product, if $H_s \in \mathscr{H}_2(\mathbb{C}_+)$ and $H_a = \mathscr{H}_2(\mathbb{C}_-)$, $\langle H_s, H_a \rangle_{\mathscr{L}_2(\imath\mathbb{R})} = 0$.

In other words, the above decomposition and Theorem 1 state that given a model $H \in \mathscr{L}_2(\imath\mathbb{R})$, there is a stable model $H_s \in \mathscr{H}_2(\mathbb{C}_+)$ and an anti-stable model $H_a = \mathscr{H}_2(\mathbb{C}_-)$ such that $H = H_s + H_a$ and $\langle H_s, H_a \rangle_{\mathscr{L}_2(\imath\mathbb{R})} = 0$. Then the following proposition holds.

Proposition 1 (Input-output $L_\infty - L_2$ stability). *A system $H \in \mathscr{L}_2(\imath\mathbb{R})$ is (input-output $L_\infty - L_2$) stable if and only if $H \in \mathscr{H}_2(\mathbb{C}_+)$.*

The Parenchel's Theorem and the $\mathscr{L}_2(\imath\mathbb{R})$ space decomposition are the main ingredient for the proposed $\mathscr{L}_2$-MFSA procedure. These arguments are provided in the following.

4.3 Theoretical $\mathscr{L}_2$-MFSA Oriented Arguments

The proposed arguments are based on the results stated in [20] and recalled in Propositions 2, 3 and 4, and finally in Theorem 2, providing the basis for the proposed numerical procedure. First of all, let us assume that the global minimizer $\tilde{H}$ of the $\mathscr{H}_2(\mathbb{C}_+)$ and $\mathscr{H}_2(\mathbb{C}_-)$ approximation problems exist[3]. Then, the following first result holds true.

---

[3] The $\mathscr{H}_2(\mathbb{C}_+)$ approximation problem is simply the $\mathscr{H}_2$ one, while the $\mathscr{H}_2(\mathbb{C}_-)$ stand as the same one but for $H(-s)$.

Proposition 2 ($\mathscr{L}_2$ orthogonality [20]). *If $H \in \mathscr{H}_2(\mathbb{C}_+)$ and there exists a global minimizer $\tilde{H} \in \mathscr{L}_2(\imath\mathbb{R})$ of the $\mathscr{L}_2$ approximation problem, then $\tilde{H} \in \mathscr{H}_2(\mathbb{C}_+)$. Similarly, if $H \in \mathscr{H}_2(\mathbb{C}_-)$ and there exists a global minimizer $\tilde{H} \in \mathscr{L}_2(\imath\mathbb{R})$ of the $\mathscr{L}_2$ approximation problem, then $\tilde{H} \in \mathscr{H}_2(\mathbb{C}_-)$.*

Thus, if a system H is stable, then the global minimizer $\tilde{H}$ of the $\mathscr{L}_2$ approximation problem is stable too. In the same way, if a system H is anti-stable, i.e., all its singularities are unstable, then the global minimizer $\tilde{H}$ of the $\mathscr{L}_2$ problem is anti-stable as well. This result comes from the orthogonality property of $\mathscr{H}_2(\mathbb{C}_-)$ and $\mathscr{H}_2(\mathbb{C}_+)$ spaces.

Let us now denote by $\tilde{H}_k$, the sequence of models of order k and consider the case where the initial model H is stable, then the following propositions hold:

Proposition 3 (Unstable approximate sequence of stable model [20]). *Given a stable model $H \in \mathscr{H}_2(\mathbb{C}_+)$, there exists a sequence of k-th order unstable models $\tilde{H}_k \in \mathscr{L}_2(\imath\mathbb{R})\backslash\mathscr{H}_2(\mathbb{C}_+)$, $k \in \mathbb{N}^*$, such that, when $k \to \infty$, $||H - \tilde{H}_k||_{\mathscr{L}_2} \to 0$.*

Thus, the set $\mathscr{H}_2(\mathbb{C}_+)$ is not an open set of $\mathscr{L}_2(\imath\mathbb{R})$. As a consequence, it is always possible to approximate a stable model H by an unstable one of order k while decreasing the mismatch error $||H - \tilde{H}_k||_{\mathscr{L}_2}$. Similarly, let us now consider the case where the initial model H both has stable and unstable modes.

Proposition 4 (Unstable approximate of unstable model [20]). *Given an unstable model $H \in \mathscr{L}_2(\imath\mathbb{R})\backslash\mathscr{H}_2(\mathbb{C}_+)$, there exists $\varepsilon > 0$ such that the ball $B_\varepsilon(H)$ defined as*

$$B_\varepsilon(H) = \left\{ \tilde{H}_k \in \mathscr{L}_2(\imath\mathbb{R}) \; \big| \; ||H - \tilde{H}_k||_{\mathscr{L}_2} < \varepsilon \right\}, \tag{21}$$

satisfies $B_\varepsilon(H) \subset \mathscr{L}_2(\imath\mathbb{R})\backslash\mathscr{H}_2(\mathbb{C}_+)$.

Thus, the set of unstable systems $\mathscr{L}_2(\imath\mathbb{R})\backslash\mathscr{H}_2(\mathbb{C}_+)$ is an open set of $\mathscr{L}_2(\imath\mathbb{R})$. Moreover, by fixing an arbitrarily small ε, it is always possible to find a $\tilde{H}_k$ that is unstable too. Based on the above propositions, let us now formulate the stability argument which will be invoked in order to derive the proposed numerical procedure.

Theorem 2 (Main stability argument). *Given an unstable system $H \in \mathscr{L}_2(\imath\mathbb{R})\backslash\mathscr{H}_2(\mathbb{C}^+)$, there exists $r \in \mathbb{N}^*$ for which the minimizer $\tilde{H}_k$ of order $k \in \mathbb{N}^*$, $k \geq r$, obtained from the $\mathscr{L}_2$-approximation problem is also unstable.*

Since Proposition 4 states that if a system $\tilde{H}_k$ is sufficiently close to an unstable system in the $\mathscr{L}_2(\imath\mathbb{R})$-norm, it is also unstable. Since, the subspace of rational finite LTI systems function is dense in $\mathscr{L}_2(\imath\mathbb{R})$, for a given unstable LTI system $H \in \mathscr{L}_2(\imath\mathbb{R})\backslash\mathscr{H}_2(\mathbb{C}^+)$, a sequence $\tilde{H}_k$ of systems of order $k \in \mathbb{N}$ which satisfies the $\mathscr{L}_2$ approximation problem, will converge to H. Thus, due to Proposition 4, there exists an order $r \in \mathbb{N}^*$ such that if $k \geq r$, $\tilde{H}_k$ will be unstable as well.

In other words there exists an approximation order $k \geq r$ such that if the original system H is unstable, the approximated one $\tilde{H}$ is unstable too. Moreover, if one has found the global $\mathscr{L}_2$ minimizer of the approximation problem of order r, it will be

stable if the original model is stable, due to Proposition 2, and it will be unstable if the original model is unstable, due to Theorem 2.

In [20], these arguments are used to derive a procedure based on the TF-IRKA algorithm [3], combined with a search of the approximation order r. This last procedure did provide quite good results but the search for an adequate order r was complex. Moreover, the TF-IRKA is an $\mathscr{H}_2(\mathbb{C}_+)$-oriented procedure and its validity in the $\mathscr{L}_2(\imath\mathbb{R})$ function space is limited to models where the stable and anti-stable part is known [16].

Here, the $\mathscr{H}_2$-optimal interpolatory conditions are released and one now considers the interpolatory conditions embedded in the Loewner framework instead. One major benefit of such a trade stands in the selection of the approximating order r, which may be automatically selected thanks the Loewner matrix rank computation. By coming back to the $\mathscr{L}_2$-MFSA procedure defined in Algorithm 1, step 2 provides a quite simplifying solution, where the dimension r is automatically determined. Then, following Propositions 3 and 4, it appears quite natural that, after approximating the interpolated model $\tilde{H}$ with $\tilde{H}_s$ using the methodology proposed by [15], the $\mathscr{L}_2$ distance evaluation is applied. Indeed, as

- from a stable model it is always possible to find an unstable one which minimizes the $\mathscr{L}_2$ mismatch problem. If, based on an unstable approximation, a stable model with the same complexity (order) can be obtained without affecting the $\mathscr{L}_2$-norm, then the interpolated model is stable (as the original one).
- from an unstable model, its global minimizer in the $\mathscr{L}_2$ sense should be unstable as well. Applying a stable approximation will lead to a large $\mathscr{L}_2$ mismatch. Then, one may confirm that the original model is unstable, as is its rational approximation.

5 Application

The proposed methods herein are applied to a a generic example of a medium size business jet for which a detailed model of the rigid body dynamics, aerodynamics as well as structural dynamics is available. The model of the aircraft is divided into subsections, i.e., the front section, a middle section including the wings, and a rear section with the elevators and the aircraft's tail, so that the effect of an incoming gust can be realistically modeled. Each section features three gusts inputs, one for the actual gust and its two derivatives in time, which are required to realistically model the unsteady aerodynamics. Having gust inputs for each aircraft sections enables, for example, a delayed injection of a gust for each part so that the gust can hit the different sections of the aircraft one after the other and mimic a realistic behavior.

To compute and compare loads with and without load alleviation controller an aircraft model with about 300 states is available. Besides the basic aircraft dynamics, the model also includes realistic actuator and sensor models as well as a baseline control law, providing adequate handling qualities to the pilot. The control inputs to the open loop aircraft model are the commands of the elevator, the inner ailerons

and the outer ailerons. The gust impact on the model is characterized by nine inputs describing the position, velocity and acceleration impact at three different locations along the fuselage. As measured signals for feedback control, the pitch rate, the load factor, and the angle of attack are provided. The provided baseline controller only commands the elevator, while the load alleviation controller shall use the ailerons symmetrically to alleviate the bending moments due to gusts. In the following the derived tool-chain is applied to design the gust load alleviation system for the available aircraft model.

5.1 Model Approximation

Ten LTI aircraft models, each of about 300 states, linearized on ten different trim points in the flight envelope (i.e., different speeds and altitudes) and in the weight and balance domain (i.e., different masses and center of gravity positions) are available. The high number of states and the nine gust inputs make the estimator and control design challenging. Thus the idea is to reduce the state dimension and the number of disturbance inputs. Considering the disturbance estimator and control design, it is preferable to use a single disturbance input. The nine disturbance inputs are used in the available simulation to model a *single* gust hitting three different sections (front, middle, rear) of the aircraft one after another. The derivatives of the three gust input positions are required to consider the unsteady aerodynamics. Consequently, the second and third set of gust inputs are equal to the first one but delayed by a fixed time delay. Thus, mathematically the second and third set of inputs can be derived by simply delaying the first one. Additionally, the velocity and acceleration of the first gust input can be derived by derivative action on the first gust input position, finally reducing the gust inputs to a single one. After these modifications, the resulting models now embed two internal delays (denoted τ_1 and τ_2, related to the velocity of the aircraft) and have a rank deflective descriptor form. These internal delays are explained by the use of exact delay actions applied on the exact derivative terms. Thus, the linear time-invariant dynamical systems can be represented by a first order descriptor realizations with n_u inputs (including one single gust input), n_y outputs, n_x internal variables, and the two internal delays. The $N = 10$ models are given by sets of differential and algebraic equations for $i = 1, \ldots, N$ by

$$
\begin{aligned}
E^{(i)}\dot{x}^{(i)}(t) &= A_0^{(i)}x(t) + A_1^{(i)}x(t - \tau_1) + A_2^{(i)}x^{(i)}(t - \tau_2) + B^{(i)}u(t) \\
y^{(i)}(t) &= C^{(i)}x^{(i)}(t),
\end{aligned}
\tag{22}
$$

with the rank defective matrix $E^{(i)}$, the internal variables $x^{(i)}(t) \in \mathbb{R}^{n_x} := \mathscr{X}$, and the input and output functions $u(t) \in \mathbb{R}^{n_u} := \mathscr{U}$ and $y^{(i)}(t) \in \mathbb{R}^{n_y} := \mathscr{Y}$, respectively. $E^{(i)}, A_0^{(i)}, A_1^{(i)}, A_2^{(i)} \in \mathbb{R}^{n_x \times n_x}$, $B^{(i)} \in \mathbb{R}^{n_x \times n_u}$ and $C^{(i)} \in \mathbb{R}^{n_y \times n_x}$ are constant matrices. Note, we assume equivalent time delays τ_1 and τ_2 for all ten models.

The matrix pencil is regular if the matrix $A_0^{(i)} + A_1^{(i)}e^{-\tau_1\lambda} + A_2^{(i)}e^{-\tau_2\lambda} - \lambda E^{(i)}$ is non-singular for some finite $\lambda \in \mathbb{C}$ and a (τ_1, τ_2) couple. In this case, the associated

transfer functions are

$$H^{(i)}(s) = C^{(i)}\left(sE^{(i)} - A_0^{(i)} - A_1^{(i)}e^{-\tau_1 s} - A_2^{(i)}e^{-\tau_2 s}\right)^{-1}B^{(i)} + D^{(i)}. \qquad (23)$$

Obviously, due to the presence of delays in the dynamical part of the equations, the resulting model is now of infinite dimension. To cope with this, first an exact stable Loewner interpolation of this infinite-dimensional model by a finite order one is performed as discussed in Sect. 2.1. This leads to a large scale descriptor model of dimension n, which exactly interpolates the infinite-dimensional models H, with $\tilde{H}(s)$, of the form

$$\tilde{H}^{(i)}(s) = \tilde{C}^{(i)}\left(s\tilde{E}^{(i)} - \tilde{A}^{(i)}\right)^{-1}\tilde{B}^{(i)}. \qquad (24)$$

Now, this finite-order models (e.g. with a finite number of eigenvalues) can be readily approximated using any (frequency-limited) $\mathscr{H}_2$ oriented model approximation techniques as discussed in Sect. 2.2 and further presented in [10, 32, 21]. This leads to reduced order models with dimension $r \ll n$, as,

$$\hat{H}^{(i)}(s) = \hat{C}^{(i)}\left(s\hat{E}^{(i)} - \hat{A}^{(i)}\right)^{-1}\hat{B}^{(i)} \qquad (25)$$

which minimize the (frequency-limited) mismatch error. Finally, the 10 aircraft models each of about 300 states with nine disturbance inputs have been approximated with ten models each of order $r = 25$ with a single disturbance input. These reduced models can now be used to design the disturbance estimator.

5.2 Gust Load Alleviation System

The two degrees of freedom gust load alleviation system consists of the disturbance estimator O designed with the approaches in Sect. 3 and a feedback control law $C_{\Delta\xi}$ as schematically illustrated in Fig. 2. In this illustration the plant G includes the aircraft dynamics as well as sensor and actuator dynamics and C_η is the baseline controller to augment the longitudinal motion of the aircraft. The observer O generates the gust estimate $\tilde{d}$ of the unknown input d, using the available measurements and control inputs. The estimated gust is feed back to the controller $C_{\Delta\xi}$ which generates the additional deflections $\Delta\xi_i$ and $\Delta\xi_o$ on the inner and outer ailerons, respectively. Note, that these generated symmetric commands $\Delta\xi_i$ $\Delta\xi_o$ are added to the asymmetric aileron commands ξ_i and ξ_o for controlling the lateral axis of the aircraft (not depicted in the figure). Also note that no extra surface are used to alleviate the gusts. Readers interested in such approached are referred to [23, 22].

For the design of the estimator O the ten reduced order models derived in Sect. 5.1 are used and the the presented methods in Sect. 3 are applied. The design models feature 25 states, three control inputs, namely elevator, symmetric inner aileron and symmetric outer aileron position, one gust input and the two measurable outputs, i.e., pitch rate and the load factor. For the ten available aircraft models, ten disturbance estimators are derived and the common structure is extracted. A com-
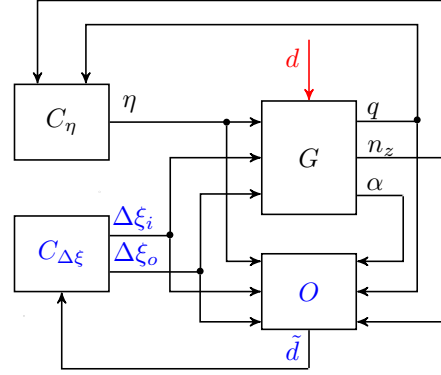
Fig. 2 Closed loop structure including aircraft dynamics G, baseline controller C_η, disturbance estimator O, and load alleviation controller $C_{\Delta\xi}$.

mon dynamic for the ten resulting first order disturbance estimators is chosen at 0.1 s, i.e., a pole at -10. This value allows a fast estimation of the incoming disturbance. Finally, applying the optimization step presented in Sect. 3.2.2 results in the disturbance estimator O with the state space realization

$$
\begin{aligned}
\dot{x}_e &= -10x_e + B_e \left[q\ n_z\ \alpha\ \eta\ \xi_i\ \xi_o \right]^T \\
\tilde{d} &= \quad x_e + D_e \left[q\ n_z\ \alpha\ \eta\ \xi_i\ \xi_o \right]^T,
\end{aligned}
\tag{26}
$$

with

$$
B_e = \left[-2\ 0.32\ -14.85\ 0.05\ 0.07\ 0.023 \right]
$$
$$
D_e = \left[0.05\ 0\ 1.5\ 0\ 0\ 0 \right].
$$

Note that the zero elements in D_e are kept 0 during the optimization step. The zeros are common in all ten disturbance estimators determined in the preliminary design step to extract the estimator structure. The disturbance estimator is discretized for the implementation in the high-fidelity simulation model with 80 Hz using a standard Tustin approximation. The sampling rate of 80 Hz correspond to the sampling rate available in the flight control computer on the actual aircraft. Having an estimate of the gust available, the estimate is feed back to symmetric aileron deflections to counteract the gust, i.e.,

$$
\begin{bmatrix} \Delta \xi_i \\ \Delta \xi_o \end{bmatrix} = C_{\Delta\xi}\tilde{d} = \begin{bmatrix} k_{\xi_i}(s) \\ k_{\xi_o}(s) \end{bmatrix} \tilde{d}.
\tag{27}
$$

Note that only the ailerons are used to mitigate the gust loads. Due to their proximity to the center of gravity in the longitudinal direction, the ailerons induce a neglectable pitching moment. This minimizes the influence of the additional control law on the aircraft handling qualities. For this paper, constant gains $k = k_{\xi_i} = k_{\xi_o}$ between -2.5 and -0.1 have been selected, for which the stability assessment is performed next.

5.3 Stability Assessment

In this section the proposed $\mathcal{L}_2$-MFSA procedure is applied to the considered aircraft models including two internal and one output delay. Before running multiple simulations, we are interested if the closed loop including the derived observer and the feedback gain, is stable. The multiple delays model depending on the feedback gain $k = k_{\xi_i} = k_{\xi_o}$ reads as

$$H^{(i)}(s,k) = C^{(i)}\left(sE^{(i)} - A_0^{(i)} - A_1^{(i)}e^{-\tau_1 s} - A_2^{(i)}e^{-\tau_2 s} - A_3^{(i)}e^{-\tau_3 s}\right)^{-1}B^{(i)}, \qquad (28)$$

where τ_3 stands as the additional output delay caused by the acquisition chain and $k \in \mathbb{R}_-$ is the controller gain (here we use a static gain for simplicity) which will be used as tuning parameter to evaluate the closed-loop stability before time-domain simulations. Note, that the row dimension of the above matrices is around 500). Fig. 3 illustrates the results of the $\mathcal{L}_2$-MFSA when applied to (28), for different frozen values of k, between -2.5 and -0.1 (here 50 points linearly spaced are used).

With reference to Fig. 3, it appears that a gain $k < -0.7571$ will result in a large index S, meaning that the closed-loop system gets unstable. Then for $-0.6143 < k < -0.1$, the index becomes low, indicating that these values of the control gain result in a stable closed-loop. When time-domain simulations are performed (not provided herein due to confidentiality reasons) for these frozen k-values, quite similar results are obtained, confirming the functionality of the proposed analysis method. However, when k is between -0.7571 and -0.7, the stability index indicates a stable behavior although the system is actually unstable. This problem is not yet solved and additional studies are on-going to get more insight. At this point the authors consider a numerical problem caused by the large dimension of the model (28) to be the source of the issue.
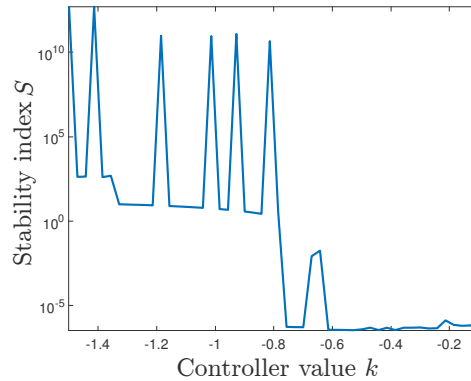

Fig. 3 Stability index S as a function of the feedback gain k, evaluated on the large-scale delayed equation (28).

5.4 Simulation-Based Load Verification

The developed gust load alleviation system is verified using a non-linear simulation model of the business jet. It features the full order aircraft model, detailed sensor models with anti-aliasing filters, non-linear actuator models, and the baseline control law for the longitudinal axis. The whole flight control system is simulated in discrete from with a sample rate of 80 Hz. The loads on six dedicated position on each wing can be explicitly determined. For the work herein, the wind bending moments as predominant loads for sizing the aircraft structure are analyzed. The gust scenario is an 1-cosine gust [8, 9], hitting the aircraft from the front with an upward wind velocity and making its way over the three sections of the aircraft. Gust wavelengths between 27.5 m and 46 m are considered. The corresponding vertical gust speed is a function of altitude and aircraft speed and is computed internally, lying between 10 m/s and 16.5 m/s.

To verify the disturbance estimator capability to estimate the gusts an open loop simulation is performed. Fig. 4 shows the estimated gusts in comparison to the actual gusts for all ten available trim points. The first diagram depicts the results for a wavelength of 27.5 m, the second for 34.7 m, and the third for 46 m. The wavelength of 34.7 m is chosen as it is defined to be the sizing wavelength for this aircraft. Note the changing gust amplitudes for a constant wavelength setting in the diagrams of Fig. 4. In the first diagram a common problem in gust estimation is visible: The encountered delay the gusts and their estimates results from sampling and delays in the used sensors. The gust inputs have already passed over some parts of the aircraft until its effect is visible in the sensors. For the slower gusts (second and
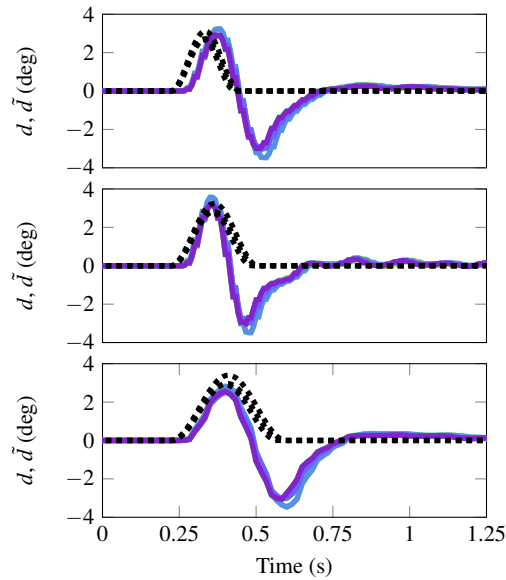

Fig. 4 Gust estimates (colored) on the ten available trim points for gust input (▪▪▪▪▪) with wavelengths of 27.5 m (first diagram), 34.7 m (second), and 46 m (third).

third diagram) a similar delay is present, however, the estimation looks better due to the reduced gust velocities. Another issue is the resulting estimate after the actual gust. While it should be zero when the 1-cos gust is over, the gust estimate shows a large undershoot. This is caused by a differentiating behavior from the gust input to the measured outputs. To counteract this behavior, one would require an integrator in the estimator. This would lead, however, to a deviating estimate over time due to the model uncertainties. Thus, the differentiating behavior is also present in the gust to gust estimate channel, leading to the undershoots in Fig. 4. The undershoot, however, does not cause any further problems as the induced moments are corrected easily by the baseline control law. Besides that, the actual estimates are rather good also in the non-linear simulation and can be used to alleviate the effect of the disturbances. Note that the baseline controller is active during all the simulations and counteracts the effect of the gust on the rigid body dynamics. This ensures that the aircraft is flying on its desired path although the gust encounter. Thus, for the gust estimator this can be interpreted as a robustness test, if the decoupling from the inputs is working. As visible in Fig. 4 the estimate are not influenced by these control inputs, which are active after about 0.75 s simulation time. The gust estimate is close to zero at this point.

Finally, the loads on the wings are computed without gust load alleviation controller and with. Based on the stability analysis results a feedback gain of $k_{\xi_i} = k_{\xi_o} = 0.6$ is selected. For each of the ten trim points five different gust wavelengths are simulated and the loads are recorded. For each trim point the maximum bending moment values encountered during the simulation over the five different gust wavelengths is depicted in Fig. 5 depending on the wing position. The same procedure is repeated with the estimator and the feedback law activated and is depicted in the second diagram of Fig. 5. The first diagram shows that the system without gust load alleviation system exactly meets the requirements on the five inboard locations points of the wing while on the most outer wing location the moments are
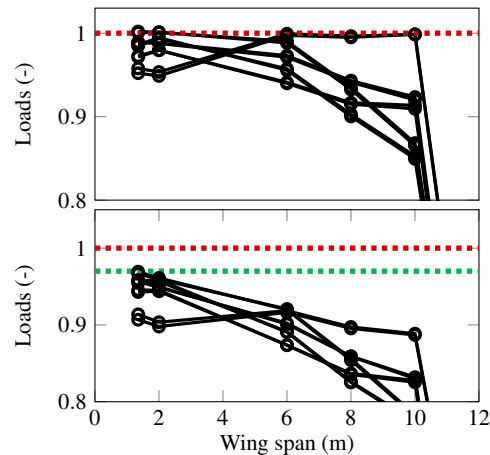

Fig. 5 Normalized loads over the wing span without (diagram 1) and with (diagram 2) load alleviation control system for the 10 available trim points.

far below the set threshold. When including the two degrees of freedom gust load alleviation system the loads are reduced by at least 3 %. This reduction occurs at the wing root for the bending moment. On the outer wing location the load reduction is even higher, reaching about 10 % between 8 m and 10 m wing span. This confirms that the developed gust load alleviation sufficiently alleviates the aircraft loads.

6 Conclusions

A tool-chain for designing wing gust load alleviation functions has been presented. High order, infinite-dimensional models with time delays are successfully approximated by low order finite-dimensional models. With these models, disturbance estimators using nullspace-based and optimization-based techniques are designed. Feeding back the estimate to the control inputs allows to efficiently alleviate the wing gust loads. Finally, a novel analytical method to validate the stability of the closed loop has been presented. The tool-chain has been successfully applied to the design of a wing gust load alleviation function for a generic businesses jet.

References

1. Antoulas, A., Lefteriu, S., Ionita, A.: Model reduction and approximation theory and algorithms, chap. A tutorial introduction to the Loewner framework for model reduction. SIAM, Philadelphia. P. Benner, A. Cohen, M. Ohlberger and K. Willcox Eds (2016)
2. Antoulas, A.C.: Approximation of Large-Scale Dynamical Systems. Advanced Design and Control, SIAM, Philadelphia (2005)
3. Beattie, C., Gugercin, S.: Realization-independent H_2-approximation. In: Proceedings of the 51st IEEE Conference on Decision and Control, pp. 4953–4958 (2012)
4. Briat, C.: LPV & Time-Delay Systems - Analysis, Observation, Filtering & Control, vol. 3. Springer-Heidelberg, Germany (2015)
5. Dalmas, V., Robert, G., Poussot-Vassal, C., Pontes Duff, I., Seren, C.: From infinite dimensional modelling to parametric reduced order approximation: Application to open-channel flow for hydroelectricity. In: Proceedings of the 15th European Control Conference. Aalborg, Denmak (2016)
6. Federal Aviation Administration: Federal Aviation Regulations Part 25, Airworthiness Standards: Transport Category (2015)
7. Fezans, N., Joos, H.D., Deiler, C.: Gust load alleviation for a long-range aircraft with and without anticipation. CEAS Aeronautical Journal pp. 1–25 (2019)
8. Flomenhoft, J.R.: Brief history of gust models for aircraft design. Journal of Aircraft **31**(5), 1225–1227 (1994)
9. Fuller, J.R.: Evolution of airplane gust loads design requirements. Journal of Aircraft **32**(2), 235–246 (1995)
10. Gugercin, S., Antoulas, A.C., Beattie, C.A.: H_2 Model Reduction for Large Scale Linear Dynamical Systems. SIAM Journal on Matrix Analysis and Applications **30**(2), 609–638 (2008)
11. International Energy Agency: Transport Energy and CO2: Moving Towards Sustainability (2009)

12. Johnston, J.: Accelerated development and flight evaluation of active controls concepts for subsonic transport aircraft. Volume 1: Load alleviation/extended span development and flight tests (1979)

13. Khalil, A., Fezans, N.: A Multi-Channel H_∞ Preview Control Approach to Load Alleviation Function Design. In: Proc. of 5th CEAS Conference on Guidance, Navigation and Control. Milano, Italy (2019)

14. Khalil, A., Fezans, N.: Performance enhancement of gust load alleviation systems for flexible aircraft using H_∞ optimal control with preview. In: Proc. of AIAA Scitech 2019 Forum. San Diego, CA, USA (2019)

15. Kohler, M.: On the closest stable descriptor system in the respective spaces RH_2 and RH_∞. Linear Algebra and its Applications **443**, 34–49 (2014)

16. Magruder, C., Beattie, C.A., Gugercin, S.: Rational Krylov methods for optimal L_2 model reduction. In: Proceedings of the 49th IEEE Conference on Decision and Control, pp. 6797–6802. Atlanta, GA, USA (2010)

17. Mayo, A.J., Antoulas, A.C.: A framework for the solution of the generalized realization problem. Linear Algebra and its Applications **425**(2), 634–662 (2007)

18. Ossmann, D., Poussot-Vassal, C.: Minimal order disturbance estimator design for aircraft load alleviation control. In: Proc. of IEEE Conference on Control Technology and Applications, pp. 787–793. Copenhagen, Denmark (2018)

19. Ossmann, D., Varga, A.: Optimization-based tuning of LPV fault detection filters for civil transport aircraft, chap. Optimization based tuning of LPV fault detection filters for civil transport aircraft, pp. 263–281. Torus Press (2013)

20. Pontes Duff, I., Vuillemin, P., Poussot-Vassal, C., Briat, C., Seren, C.: Approximation of stability regions for large-scale time-delay systems using model reduction techniques. In: Proceedings of the 14th European Control Conference, pp. 356–361. Linz, Austria (2015)

21. Poussot-Vassal, C., Vuillemin, P.: Introduction to MORE: a MOdel REduction Toolbox. In: Proceedings of the IEEE Multi-conference on Systems and Control, pp. 776–781. Dubrovnik, Croatia (2012)

22. Pusch, M.: Allocation of distributed flaps for gust load alleviation. In: Proc. of IEEE Conference on Control Technology and Applications. Mauna Lani, HI, USA (2017)

23. Pusch, M., Knoblach, A., Kier, T.: Integrated Optimization of Ailerons for Active Gust load alleviation. In: Proc. of International Forum on Aeroelasticity and Structural Dynamics. Saint Petersburg, Russia (2015)

24. Regan, C.D., Jutte, C.V.: Survey of applications of active control technology for gust alleviation and new challenges for lighter-weight aircraft. Tech. rep., NASA Dryden Flight Research Center, Edwards, CA, USA (2012)

25. Richard, J.P.: Time-delay systems: an overview of some recent advances and open problems. Automatica **39**(10), 1667–1694 (2003)

26. Seuret, A., Gouaisbaut, F.: Hierarchy of LMI conditions for the stability analysis of time-delay systems. System & Control Letters **81**, 1–7 (2015)

27. Sipahi, R., Niculescu, S., Abdallah, C., Michiels, W., Gu, K.: Stability and stabilization of systems with time delay. IEEE Control Systems Magazine **2**, 38–65 (2011)

28. Varga, A.: The nullspace method a unifying paradigm to fault detection. In: Proc. of Conference on Decision and Control. Shanghai, China (2009)

29. Varga, A.: Synthesis of robust gain scheduling based fault detection filters for a class of parameter uncertain nonlinear systems. In: Proc. of 19th Mediterranean Conference on Control and Automation. Corfu, Greece (2011)

30. Varga, A.: Solving Fault Diagnosis Problems - Linear Synthesis Techniques. Springer International Publishing (2017)

31. Vuillemin, P.: Frequency-limited approximation of large-scale LTI dynamical models. Ph.D. thesis, Onera, ISAE, Toulouse University, Toulouse, France (2014)

32. Vuillemin, P., Poussot-Vassal, C., Alazard, D.: H_2 optimal and frequency limited approximation methods for large-scale LTI dynamical systems. In: Proceedings of the 6th IFAC Symposium on Systems Structure and Control, pp. 719–724. Grenoble, France (2013)